

CR 177909

FINAL REPORT

entitled

COMPARISON OF LONG-WAVE AND SHORTWAVE
IRRADIANCES AT SATELLITE ALTITUDE WITH INTEGRATED
SCANNER MEASUREMENTS USING THE NIMBUS 7 ERB DATA SET

by

Dr. Frederick B. House
HOUSELINE, INC.
2 Crest Lane
Swarthmore, PA 19081

prepared for

Dr. H. Lee Kyle, Code 910.2
Building 22, Room 372
Goddard Space Flight Center
National Aeronautics and Space Administration
Greenbelt, MD 20771

under

Purchase Order No. S-21145-D

August 1986

(NASA-CR-1779C9) COMPARISON OF LONG-WAVE
AND SHORTWAVE IRRADIANCES AT SATELLITE
ALTITUDE WITH INTEGRATED SCANNER
MEASUREMENTS USING THE NIMBUS 7 ERB DATA SET
Final Report (Houseline, Inc.) 31 p G3/92 43373
Unclass N87-2 1834

FOREWORD

This report is submitted to the Goddard Space Flight Center, National Aeronautics and Space Administration as a deliverable item pertaining to Purchase Order No. S-21145-D, dated 4-16-84 and amended 2-25-86. The scope of work concerns a study of the scientific usefulness of the ERB data set in its present form. In view of the timing of this report relative to the processing schedule of Nimbus 7 ERB observations, emphasis is placed on a comparison of wide-field-of-view measurements with integrated scanner observations at satellite altitude. The purpose of making these comparisons is to check for the need of spectral corrections when processing the shortwave scanning radiometer data.

TABLE OF CONTENTS

<u>Section</u>	<u>Page Number</u>
COVERSHEET	i
FOREWORD	ii
TABLE OF CONTENTS	iii
1. Introduction.	1
2. Approach.	2
3. Data Processing Procedures.	3
4. Analysis of Results.	5
ATTACHED Figures 1 - 6.	7 - 28

COMPARISON OF LONG-WAVE AND SHORTWAVE IRRADIANCES AT SATELLITE ALTITUDE WITH INTEGRATED SCANNER MEASUREMENTS USING THE NIMBUS 7 ERB DATA SET

1. Introduction

The Nimbus 7 ERB data set comprises observations by three separate instrument groups: the solar monitoring radiometers, the bi-axial scanning radiometers, and the non-scanning wide-field-of-view (WFOV) radiometers. The scanning radiometers have provided an excellent set of observations for a 19-month period following launch, and the non-scanning radiometers have monitored the solar irradiance and the radiant exitance of the earth until this year -- a period of more than 7 years of continuous observations.

There are four telescopes in the cylinder arrangement that comprises the scanning radiometer assembly. Each of the telescopes employs reflection optics along the optical path, and these mirrors have non-uniform spectral reflectance properties, especially in the visible portion of the electromagnetic spectrum. On the other hand, the wide-field-of-view (WFOV) radiometers have uniform, broad-band spectral responses across the shortwave spectrum compared to those for the scanning radiometers. Thus, a careful comparison of scanning and WFOV shortwave measurements should indicate the magnitude of the spectral differences when interpreting scanner measurements.

This study performs a comparison of shortwave observations at satellite altitude to determine any obvious effects of spectral differences between the scanning and WFOV measurements.

2. Approach

The comparison of irradiances can best be performed at satellite altitude since this removes additional assumptions concerning data interpretation when estimating exitances at the top-of-the-atmosphere. Scanner observations were compiled for 10° latitude zones as described in Section 3, and then integrated to simulate irradiances observed at satellite altitude. This integration procedure convolved the shape factor for each zone with the scanner exitance and assumed no directionality functions of the emerging exitances. The weights for the shape factor depended on the view of each zone for a particular satellite position relative to that zone, and the weights varied from equator to pole, depending on the view as seen by the WFOV radiometer.

In Section 4, the results are presented in terms of irradiance differences ($E_W - E_N$) W/m^2 , that is, the difference between the WFOV and integrated scanner irradiances. These differences are computed for latitudes -70°S to 70°N , and for both shortwave and longwave irradiances, and for ascending and descending nodes of the orbit.

3. Data Processing Procedures

The ERB scanning radiometers on Nimbus 7 satellite observed reflected radiances from the earth during the 19 months of operation from November 1978 through June 1980. Usually the instrument was operated on a duty cycle of 3 days on and 1 day off. It is convenient to process observations for one 3-day period, or groups of 3-day periods, and to select those periods when the scan mode optimized the angular coverage of observations.

An estimate of reflected radiance from a target area for a particular coordinate direction (θ_e, ϕ) is determined from the time average of all radiances falling in a bin defined by angular ranges $\Delta\theta_e$ and $\Delta\phi$, centered at (θ_e, ϕ) . This study employed a 64-bin division of the hemisphere above the target area including 8 bins of view angle with $\Delta\theta_e = 10^\circ$ from 5° to 85° , and 8 bins of azimuth with an interval of $\Delta\phi = 45^\circ$ each. The azimuth bins were centered on the forward and backward scattering directions with respect to the principal plane. The zenith angle of the sun θ_0 is also an average value varying during the period of observation, the latitude range of the target (10°), and the local time of observation during satellite fly-bys. The computer code compiles observations for every 10° latitude interval from 85°N to 85°S . The selection of a 10° latitude zone is a compromise between averaging time, changing declination of the sun and adequate sampling of target areas.

Nineteen 3-day periods were chosen from the 19-month data set of scanner observations as shown in Table 1. Unfortunately, the month of October is the only missing period in the list because the compiled file was not useable for this study. When compiling radiances for each latitude zone, all measurements for a 3-day period were processed together as one group.

Table 1
Nineteen Observational Periods Employed in this Study

<u>Period Dates</u>	<u>Period Dates</u>
Nov. 20-22, 1978	
Dec. 6-8, 1978	Aug. 15-17, 1979
Jan. 7-9, 1979	Sept. 16-18, 1979
Feb. 12-14, 1979	Nov. 11-13, 1979
Mar. 4-6, 1979	Dec. 9-11, 1979
Apr. 16-18, 1979	Dec. 21-23, 1979
May 23-25, 1979	Jan 14-16, 1980
May 31-June 2, 1979	Feb. 15-17, 1980
June 16-18, 1979	Mar. 2-4, 1980
July 10-12, 1979	May 21-23, 1980

4. Analysis of Results.

The results of the study are presented in the graphs of Figures 1 through 4, and the statistical summaries in Figures 5 and 6. A separate graph is presented for each of the nineteen 3-day periods listed in Table 1. Figures 1 and 2 present longwave comparisons for descending and ascending nodes, respectively, and Figures 3 and 4 illustrate the corresponding comparisons for shortwave irradiances.

Probably, the best approach to evaluate the results is to suggest that the reader survey the graphs in the Figures. One will quickly conclude that there are variations in the differences, especially in the shortwave comparisons of Figure 4. Perhaps the question to ask is whether there are distinct differences for different latitudes zones having different basic underlying surface properties. For example, in the southern hemisphere, latitudes 50° and 60° are dominated by variable cloudiness over oceans. In contrast, latitudes 50° and 60° in the northern hemisphere are dominated by cloudiness over land masses. The subtropical regions of both hemispheres are more cloud-free than adjacent mid-latitude regions. One can pursue such arguments when viewing the comparison results.

Longwave results in Figures 1 and 2 are summarized statistically in Figure 5. The RMS difference of nineteen 3-day periods is about 2 to 3 W/m² for both ascending and descending nodes. The mean differences indicate little if any coupling with each other on ascending and descending nodes.

Shortwave results in Figures 3 and 4 are summarized statistically in Figure 6. The descending node observations are academic and illustrate the residual signal of the shortwave channel when passing into the earth's shadow at satellite sunset. The mean difference of nineteen 3-day periods on ascending node in Figure 6 are of primary concern. There is an increase of about 4 to 5 W/m^2 between 60°S and 60°N . This result is attributed to data processing procedures and should be ignored. The key question is whether there are systematic variations associated with different scene types at particular latitudes. In the opinion of the author, there is know obvious sensitivity to latitude location. The RMS differences indicate 5 to 7 W/m^2 magnitudes varying in a systematic manner. This statistic does not point to particular latitudes where there are considerably larger differences between WFOV and integrated scanner irradiances.

In summary, there appears to be know large systematic irradiance differences that may be attributed to a sensitivity to non-uniform spectral response of the scanning radiometer data when compared to the corresponding WFOV measurements.

LONGWAVE, DESCENDING NODE

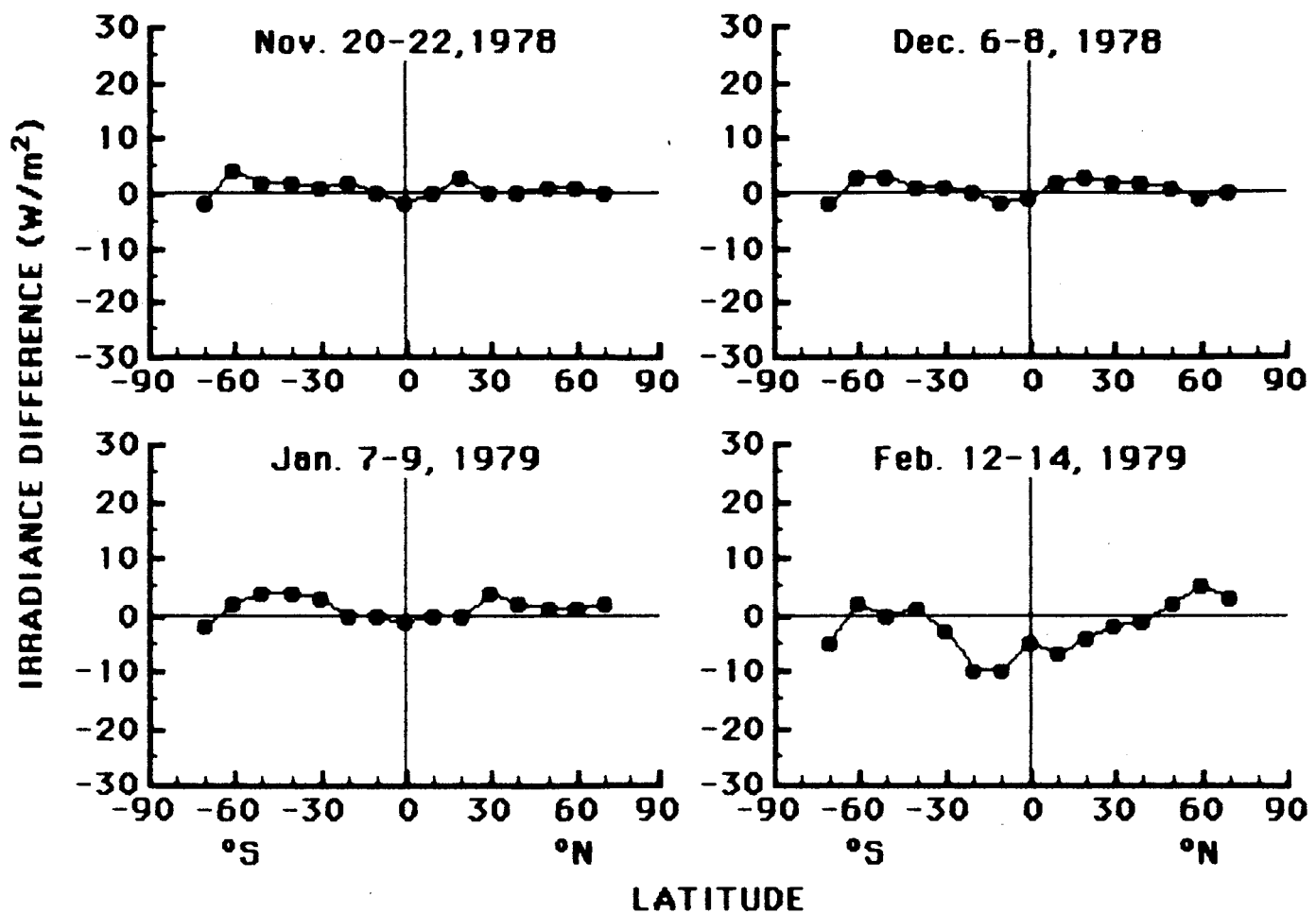


Fig. 1(a). Comparison of longwave irradiances between the WFOV non-scanning and NFOV scanning radiometers for 3-day averages of the Nimbus 7 ERB data set. The irradiance difference ($E_{WL} - E_{NL}$) W/m^2 is plotted as a function of latitude during the descending node.

LONGWAVE, DESCENDING NODE

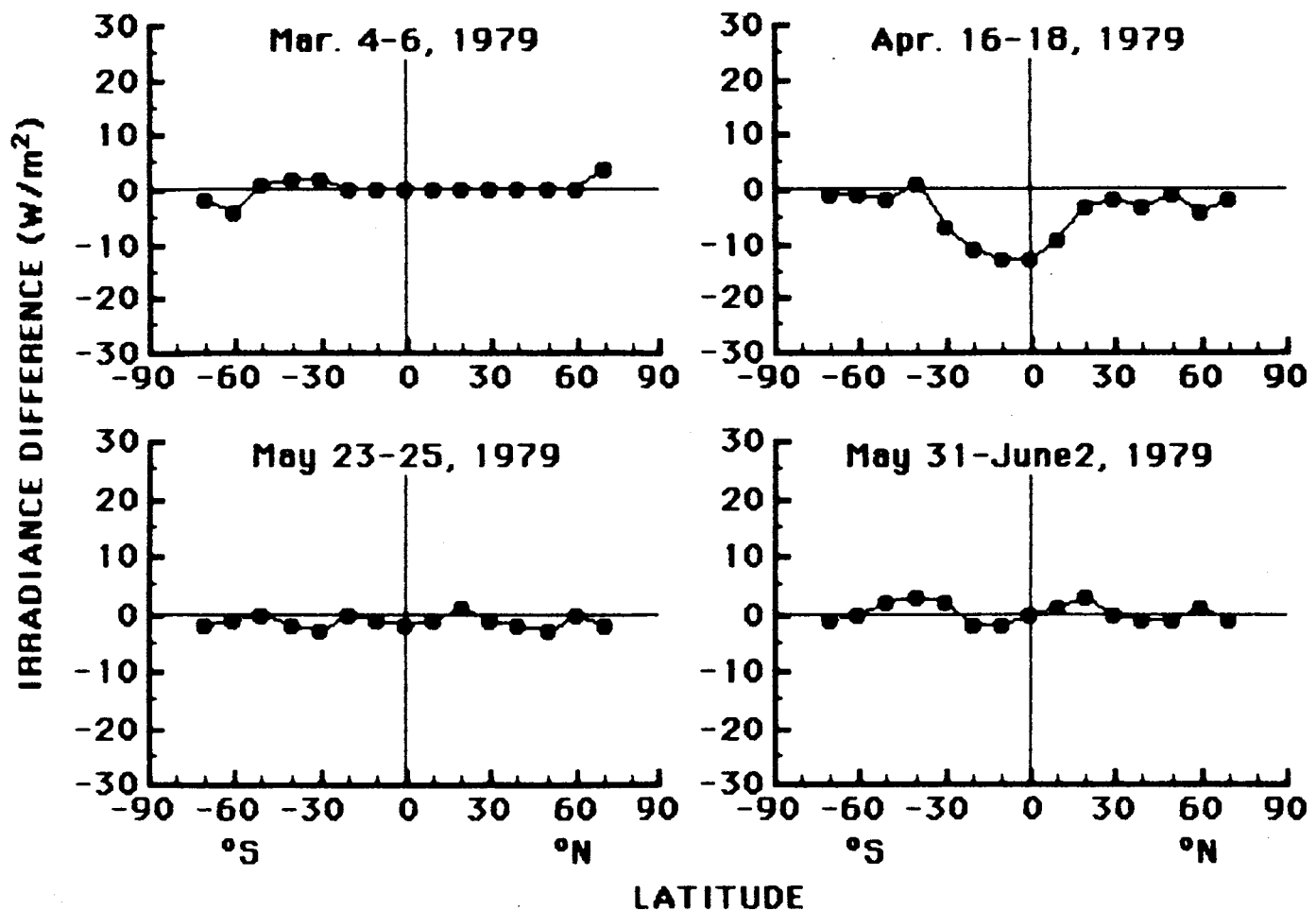


Fig. 1(b). Same as Fig. 1(a).

LONGWAVE, DESCENDING NODE

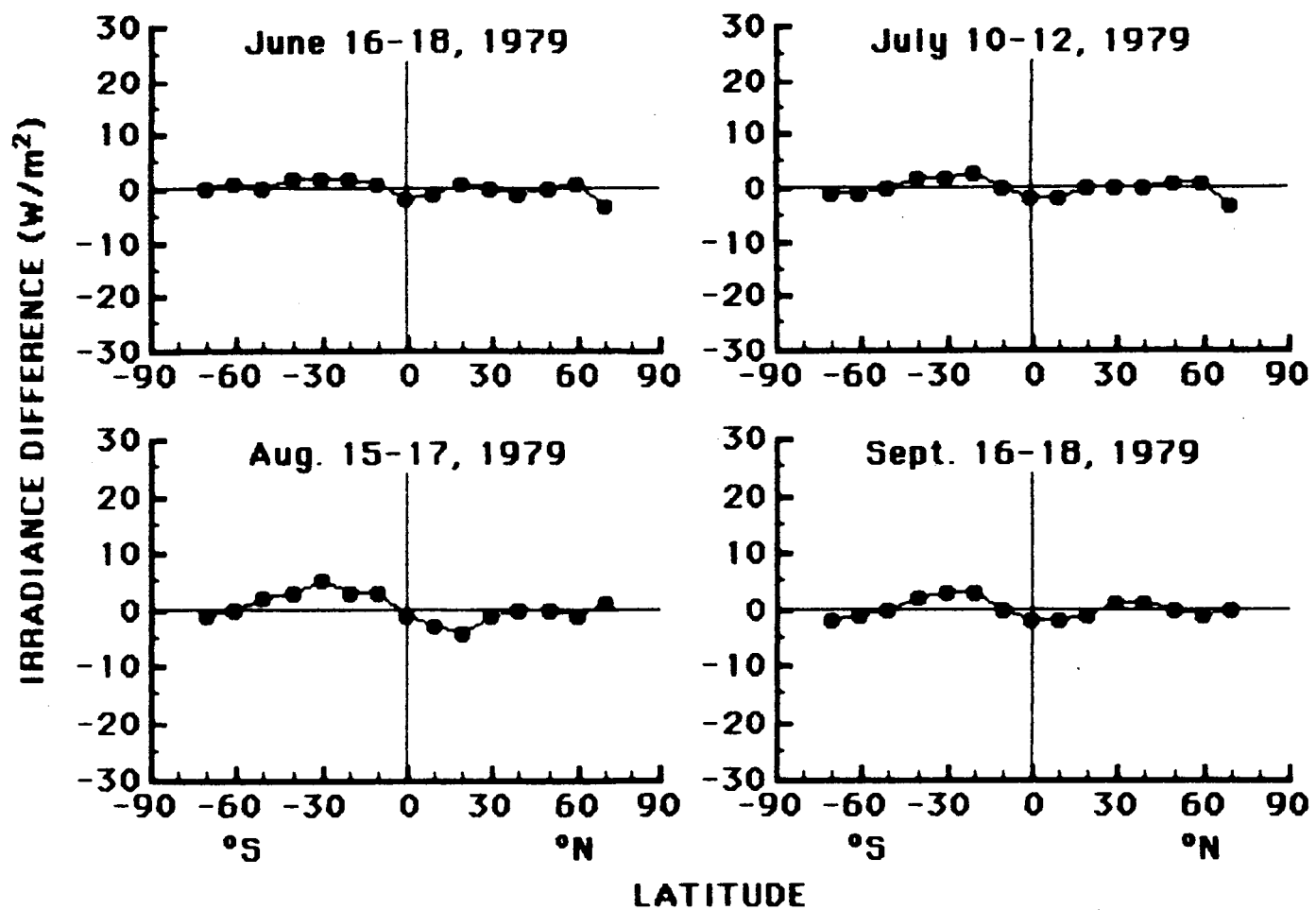


Fig. 1(c). Same as Fig. 1(a).

LONGWAVE, DESCENDING NODE

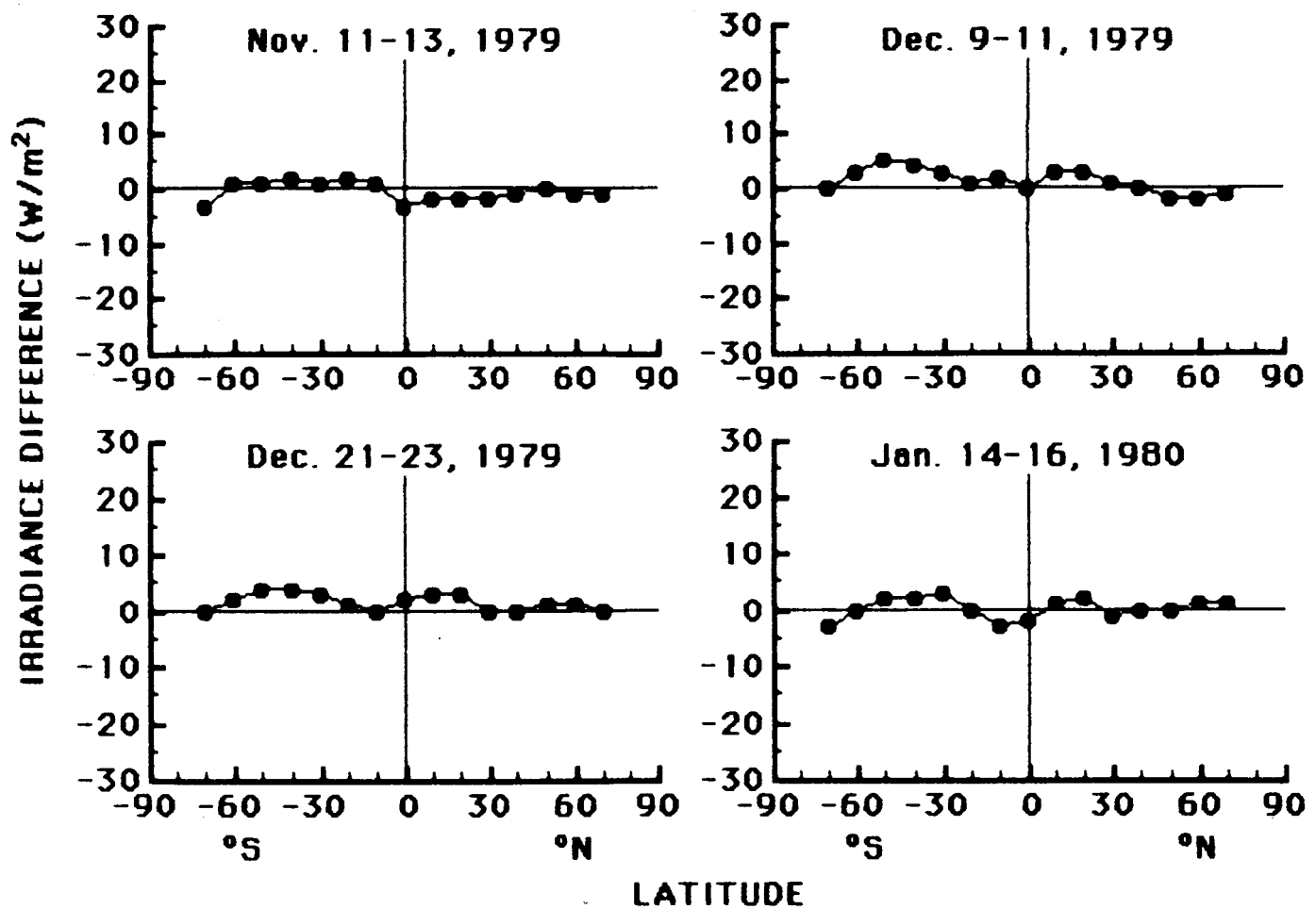


Fig. 1(d). Same as Fig. 1(a).

LONGWAVE, DESCENDING NODE

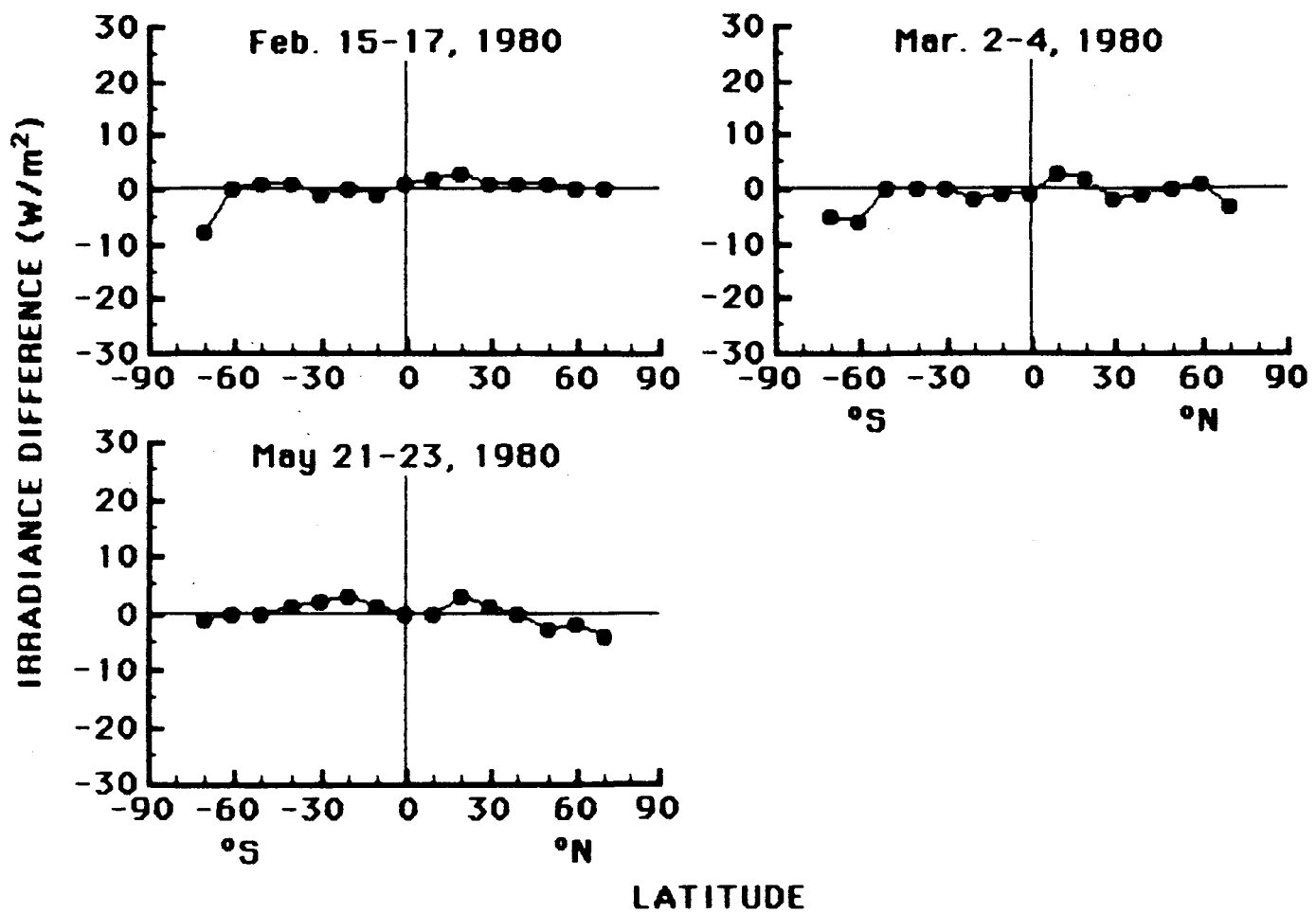


Fig. 1(e). Same as Fig. 1(a).

LONGWAVE, ASCENDING NODE

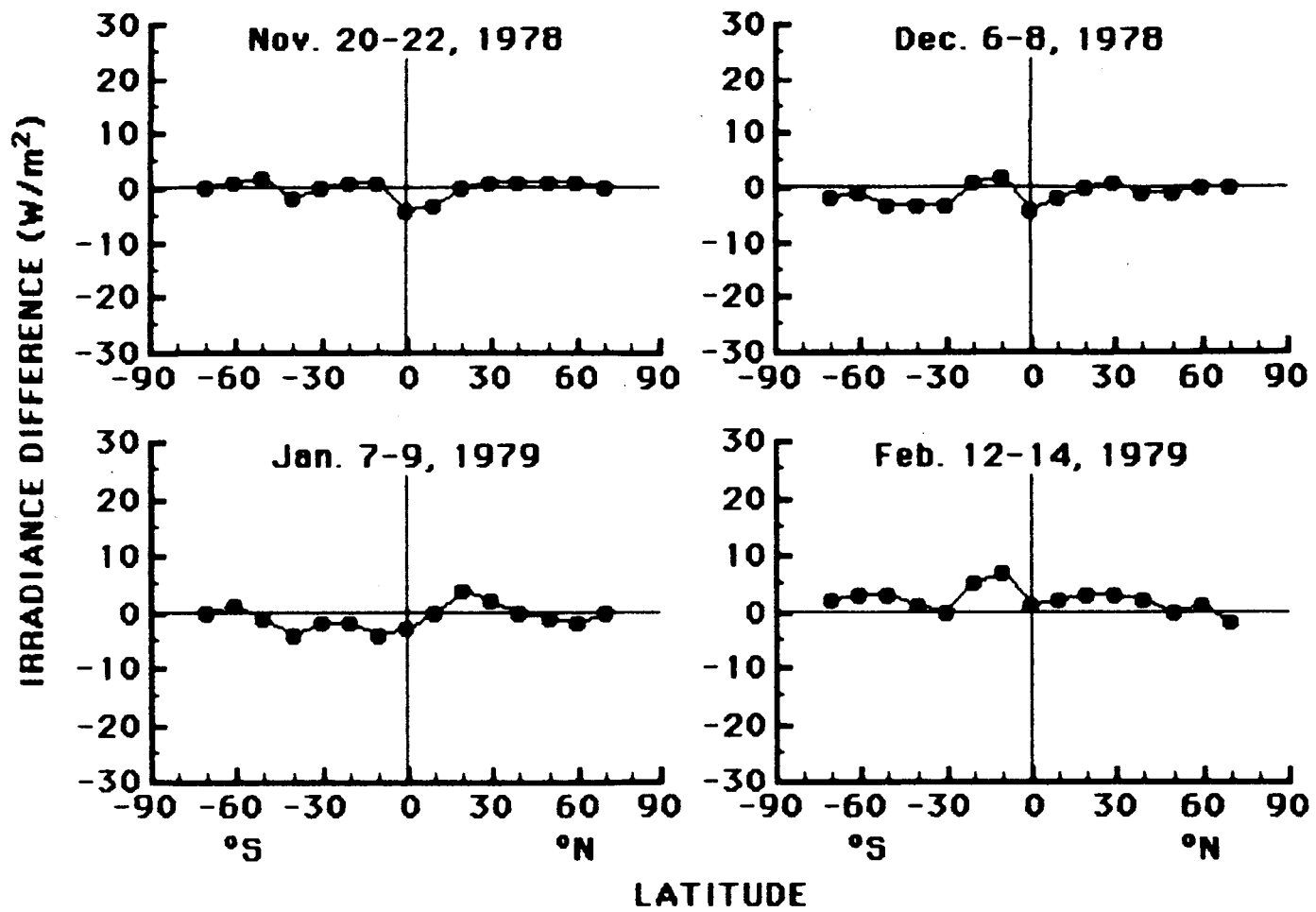


Fig. 2(a). Comparison of longwave irradiances between the WFOV non-scanning and NFOV scanning radiometers for 3-day averages of the Nimbus 7 ERB data set. The irradiance difference ($E_{WL} - E_{NL}$) W/m² is plotted as a function of latitude during the ascending node.

LONGWAVE, ASCENDING NODE

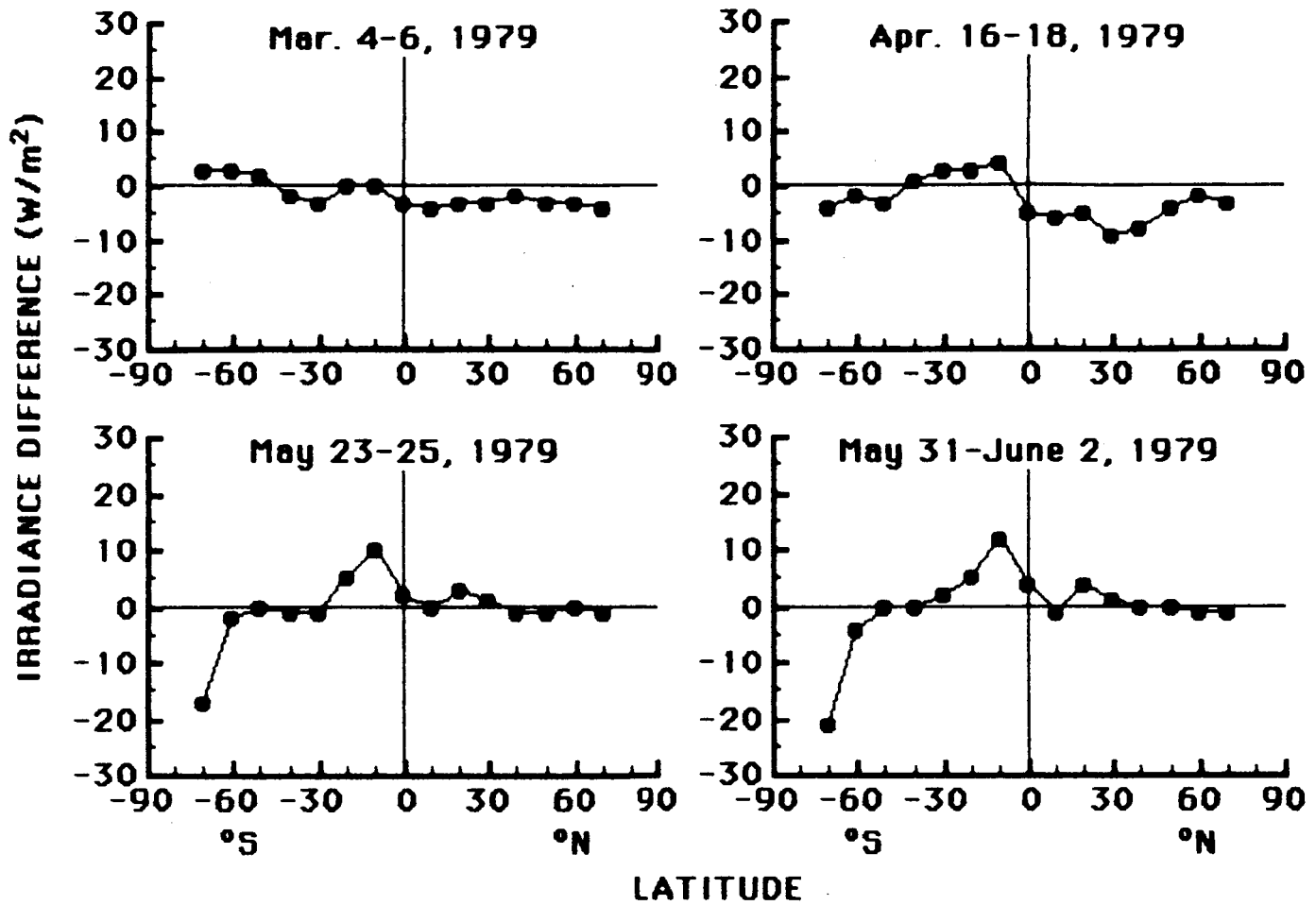


Fig. 2(b). Same as Fig. 2(a).

LONGWAVE, ASCENDING NODE

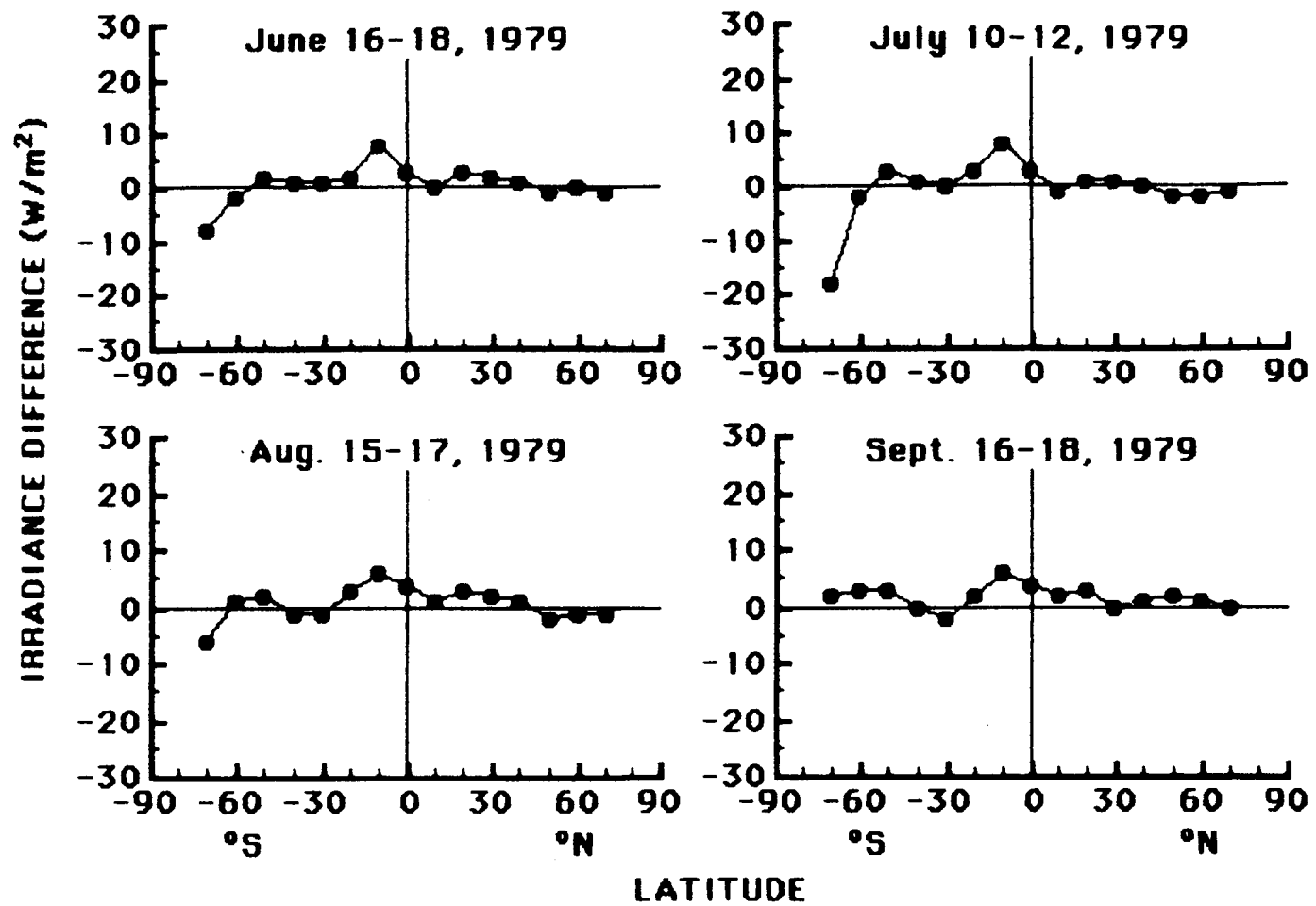


Fig. 2(c). Same as Fig. 2(a).

LONGWAVE, ASCENDING NODE

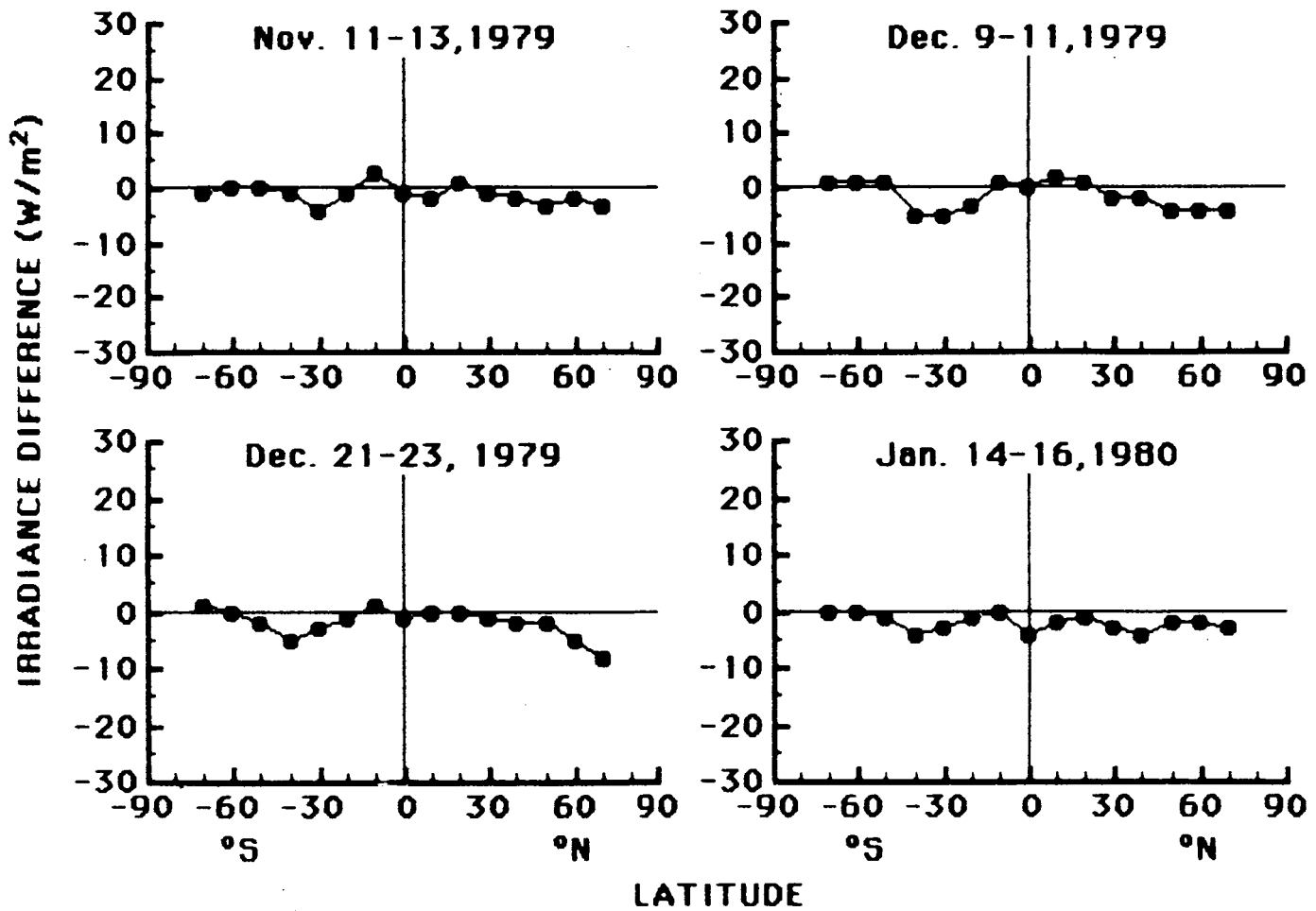


Fig. 2(d). Same as Fig. 2(a).

LONGWAVE, ASCENDING NODE

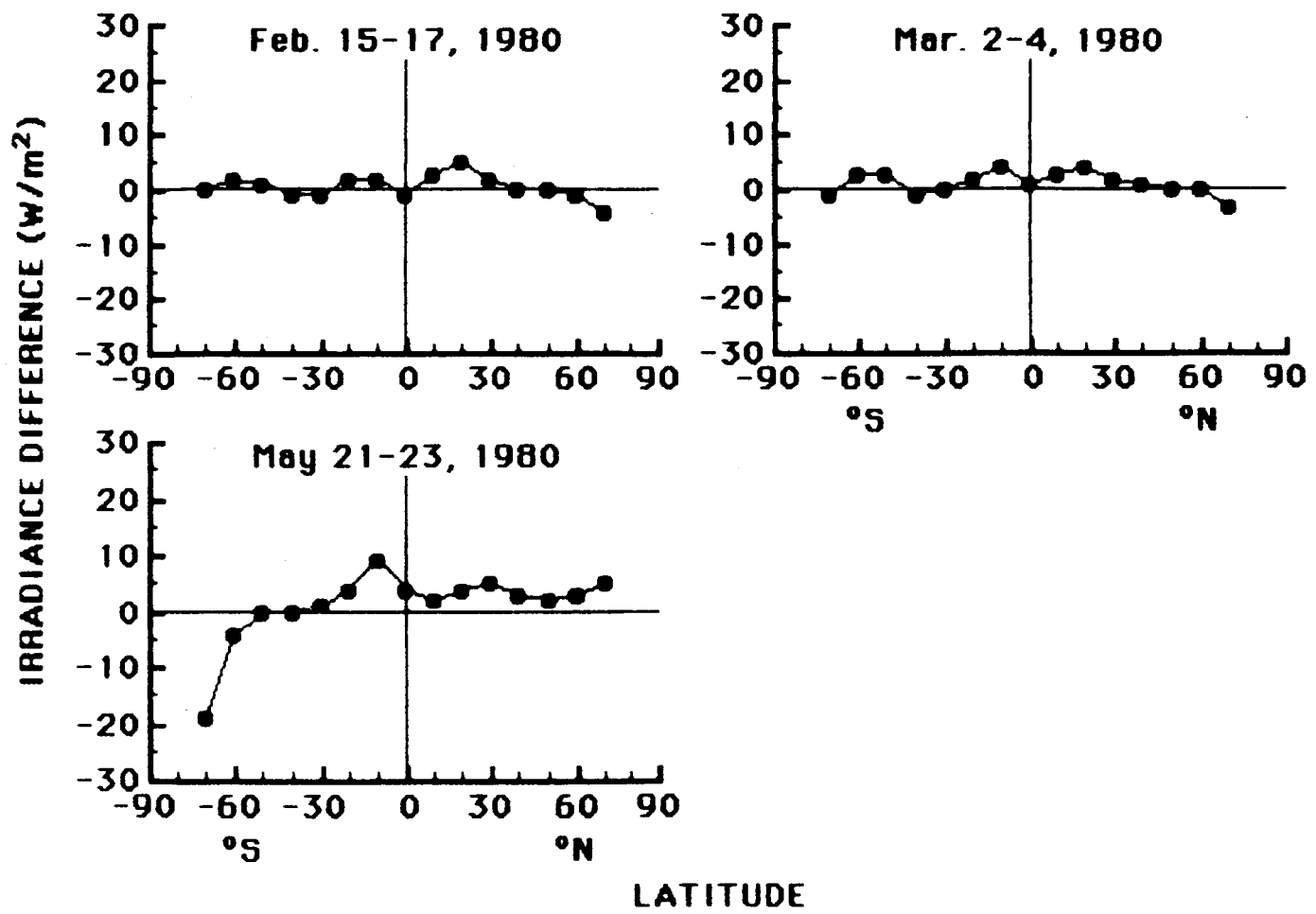


Fig. 2(e). Same as Fig. 2(a).

SHORTWAVE, DESCENDING NODE

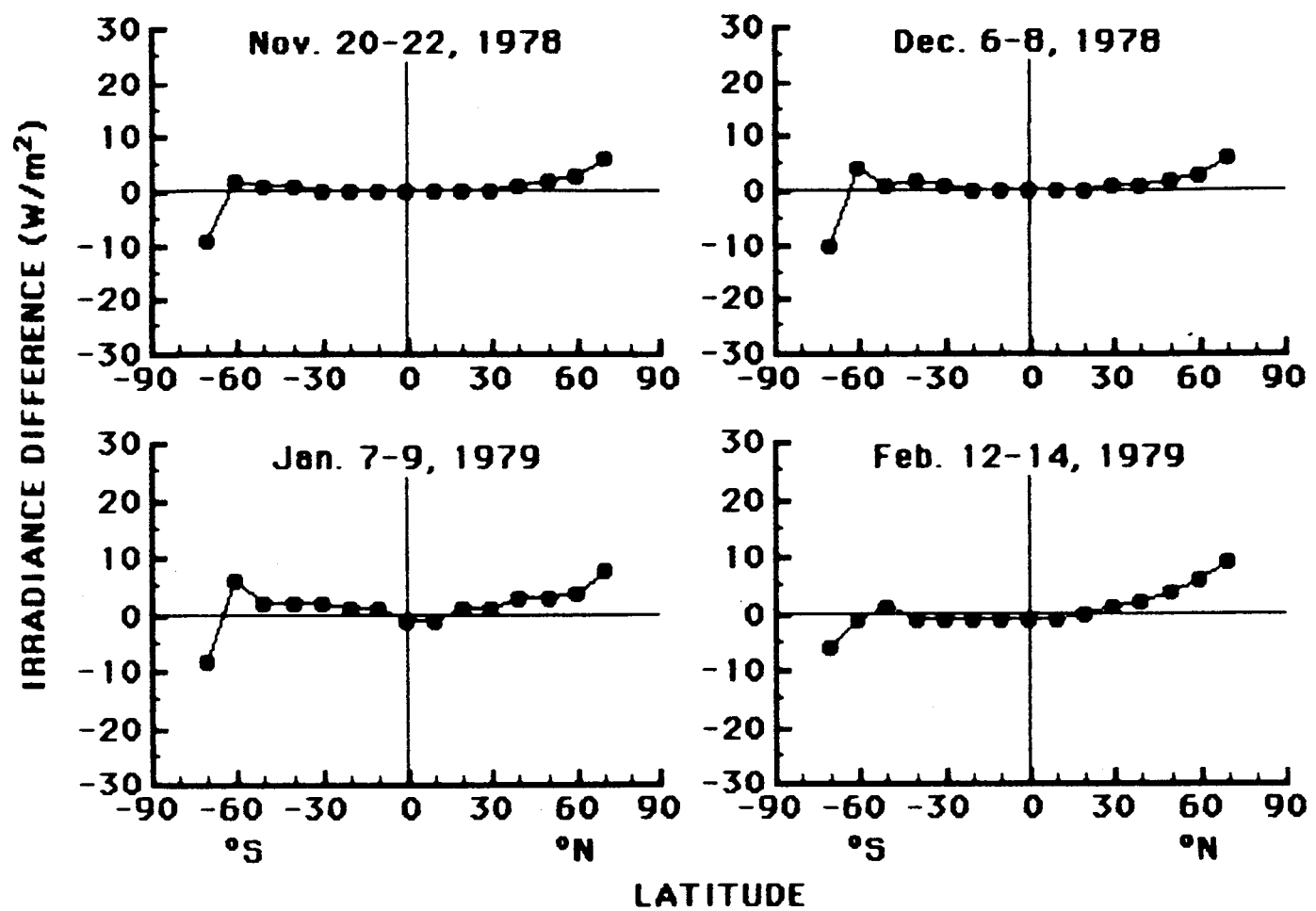


Fig. 3(a). Comparison of shortwave irradiances between the WFOV non-scanning and NFOV scanning radiometers for 3-day averages of the Nimbus 7 ERB data set. The irradiance difference ($E_{WL} - E_{NL}$) W/m² is plotted as a function of latitude during the descending node.

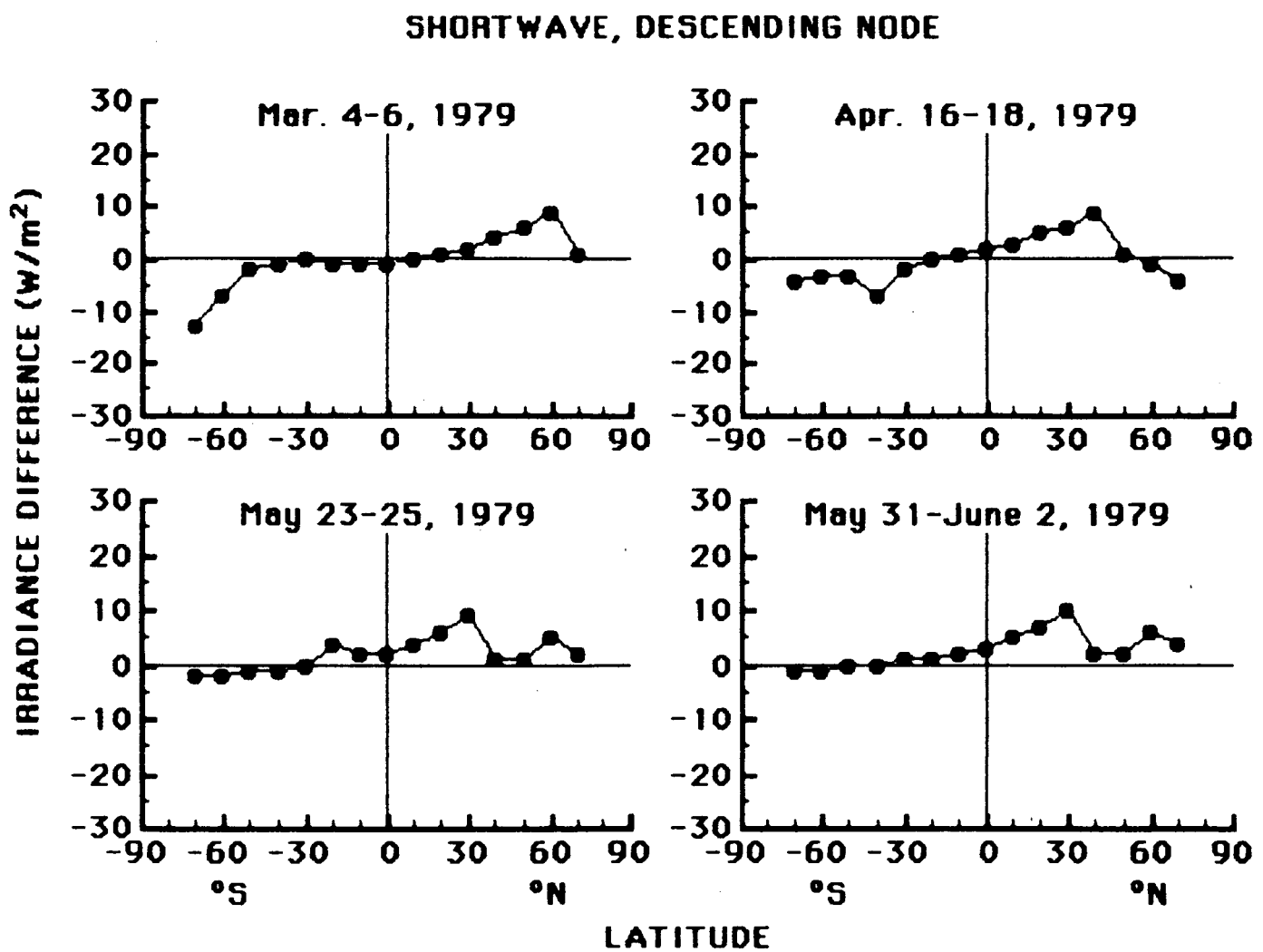


Fig. 3(b). Same as Fig. 3(a).

SHORTWAVE, DESCENDING NODE

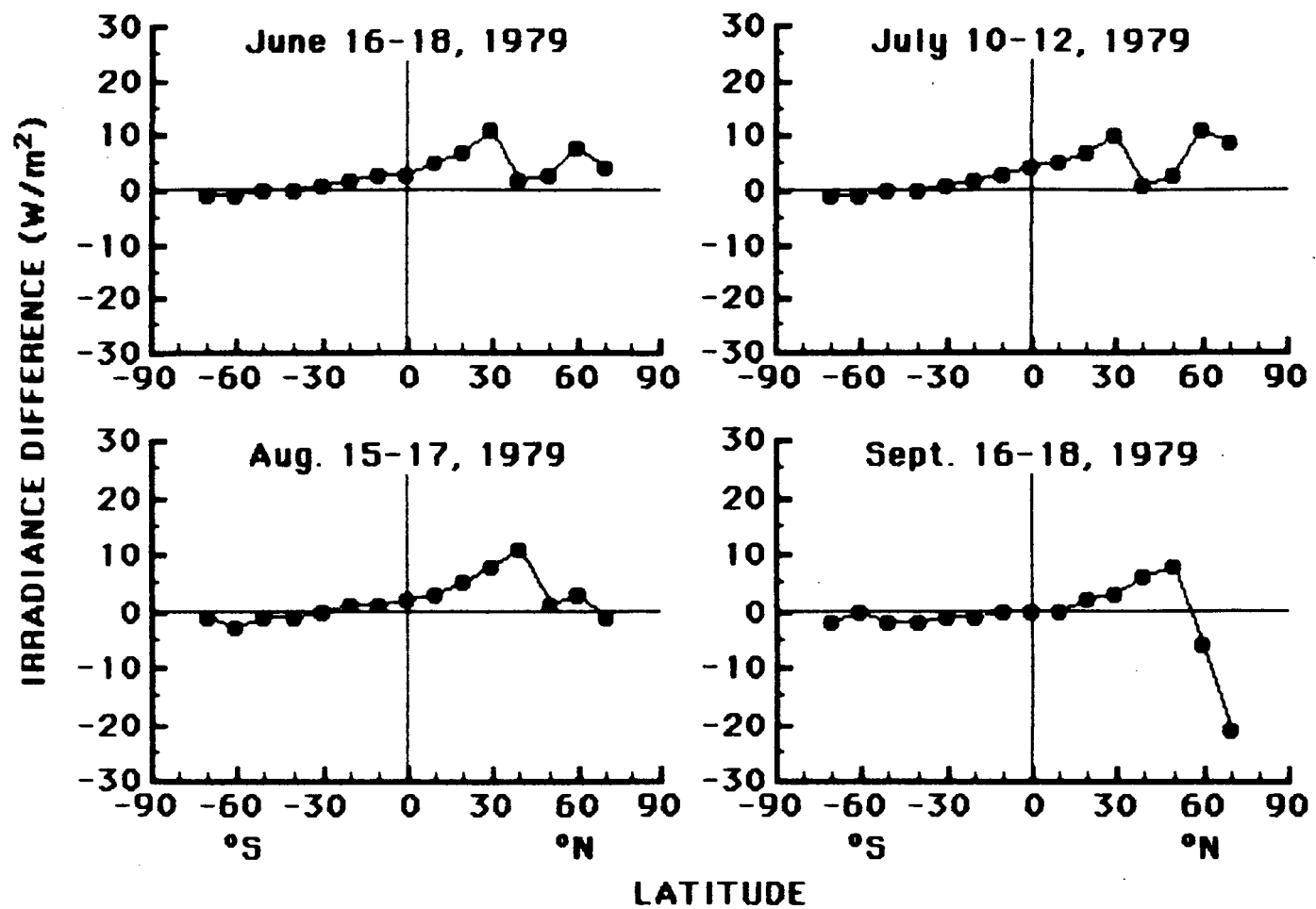


Fig. 3(c). Same as Fig. 3(a).

SHORTWAVE, DESCENDING NODE

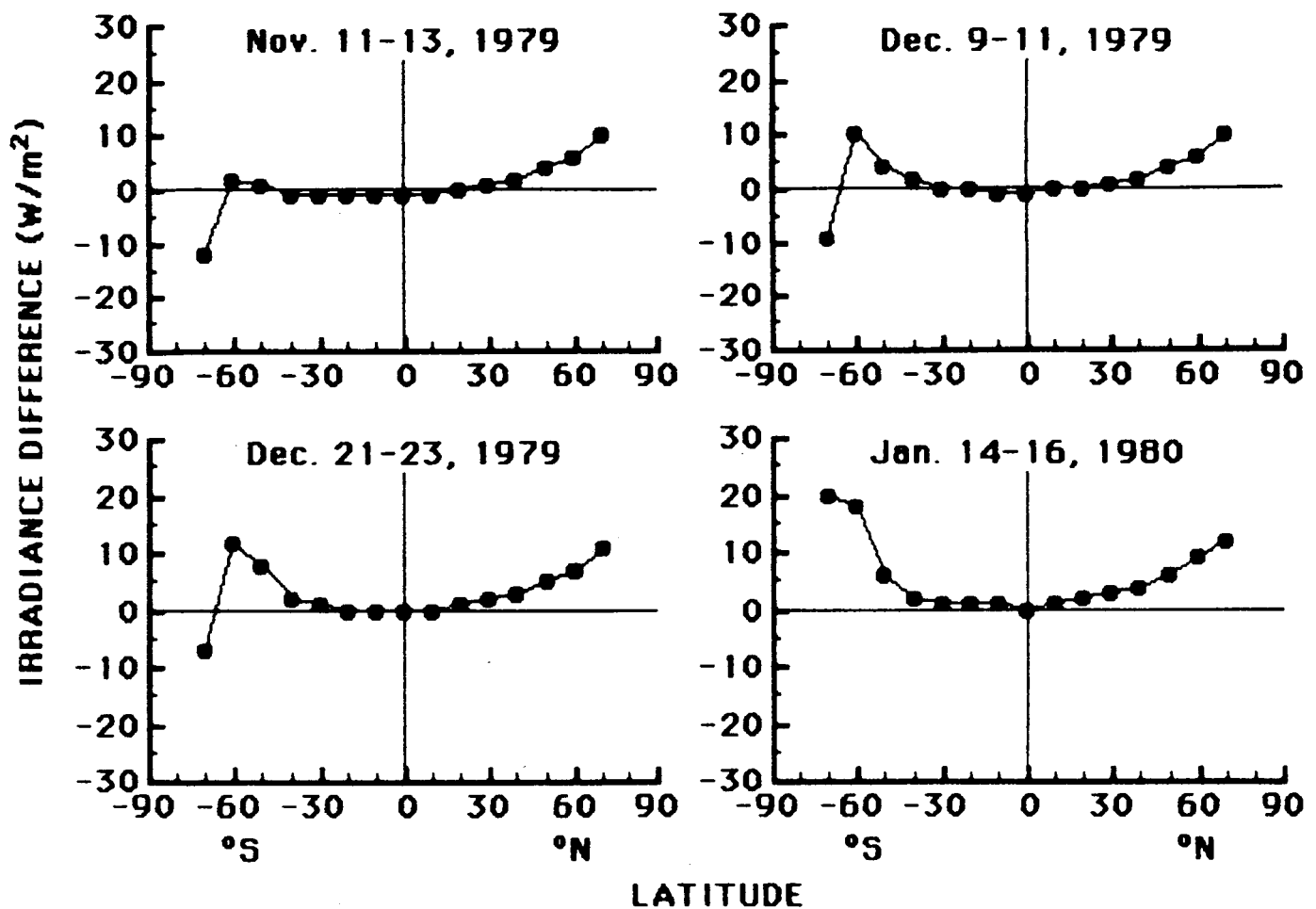


Fig. 3(d). Same as Fig. 3(a).

SHORTWAVE, DESCENDING NODE

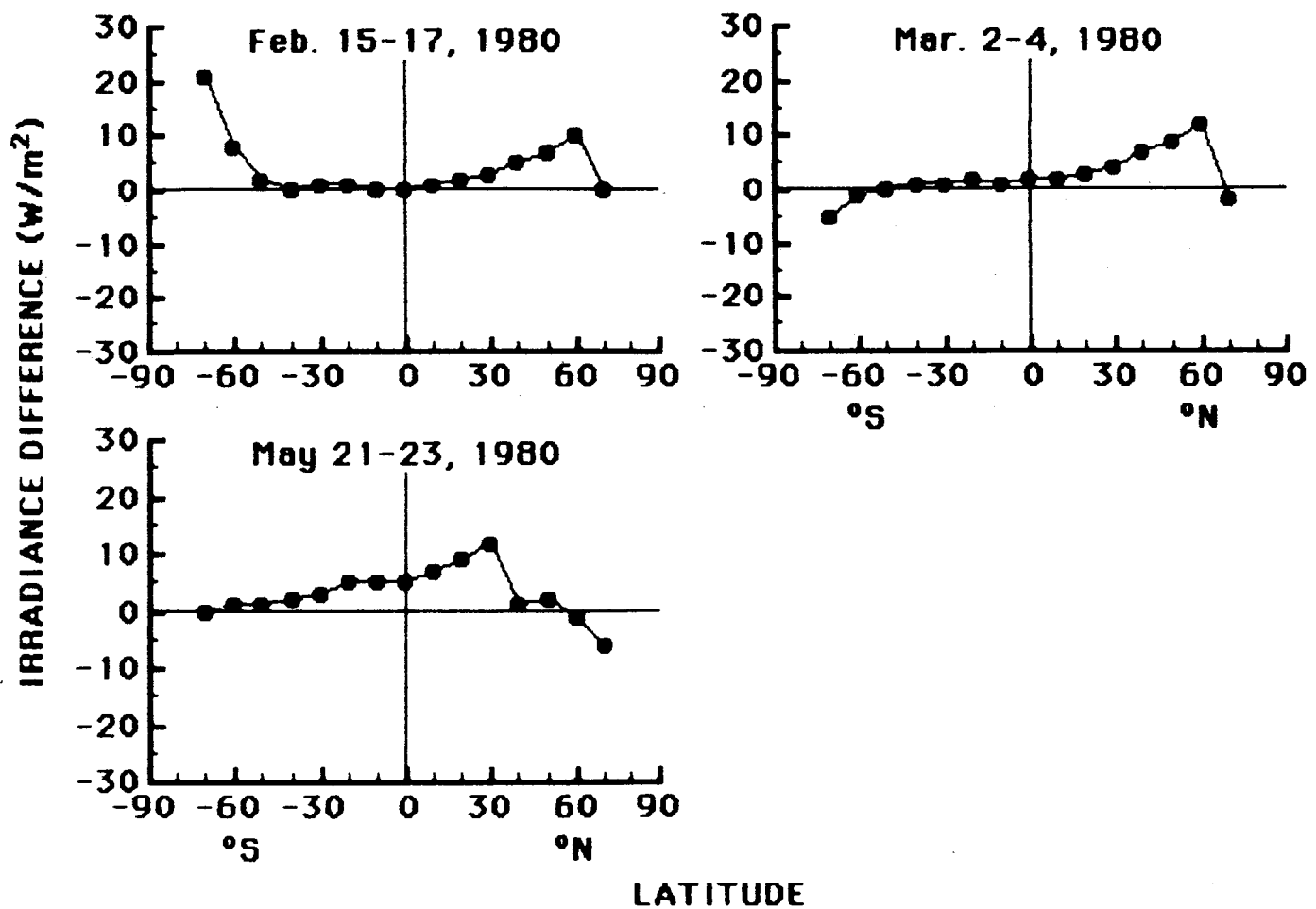


Fig. 3(e). Same as Fig. 3(a).

SHORTWAVE, ASCENDING NODE

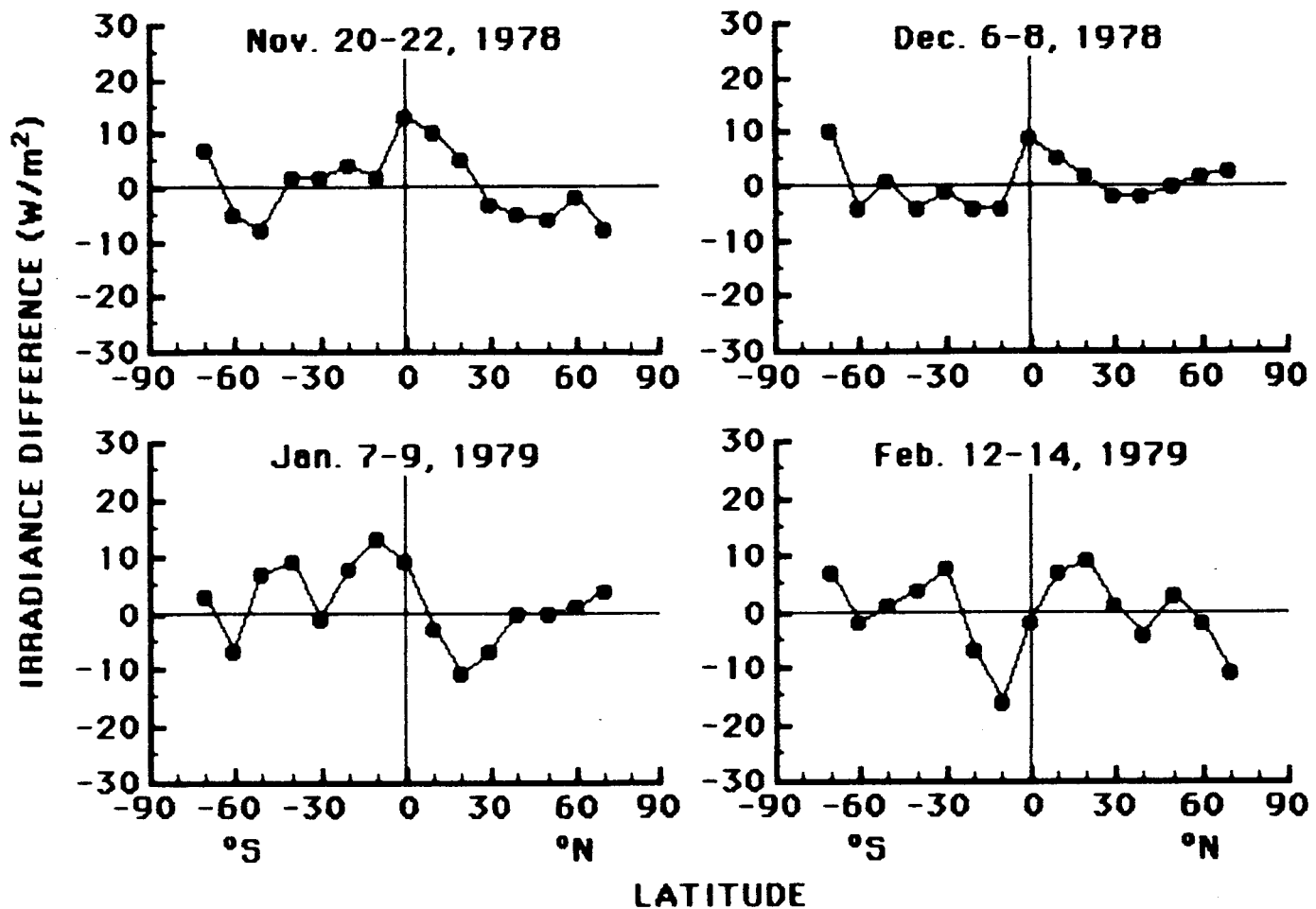


Fig. 4(a). Comparison of shortwave irradiances between the WFOV non-scanning and NFOV scanning radiometers for 3-day averages of the Nimbus 7 ERB data set. The irradiance difference ($E_{WL} - E_{NL}$) W/m² is plotted as a function of latitude during the ascending node.

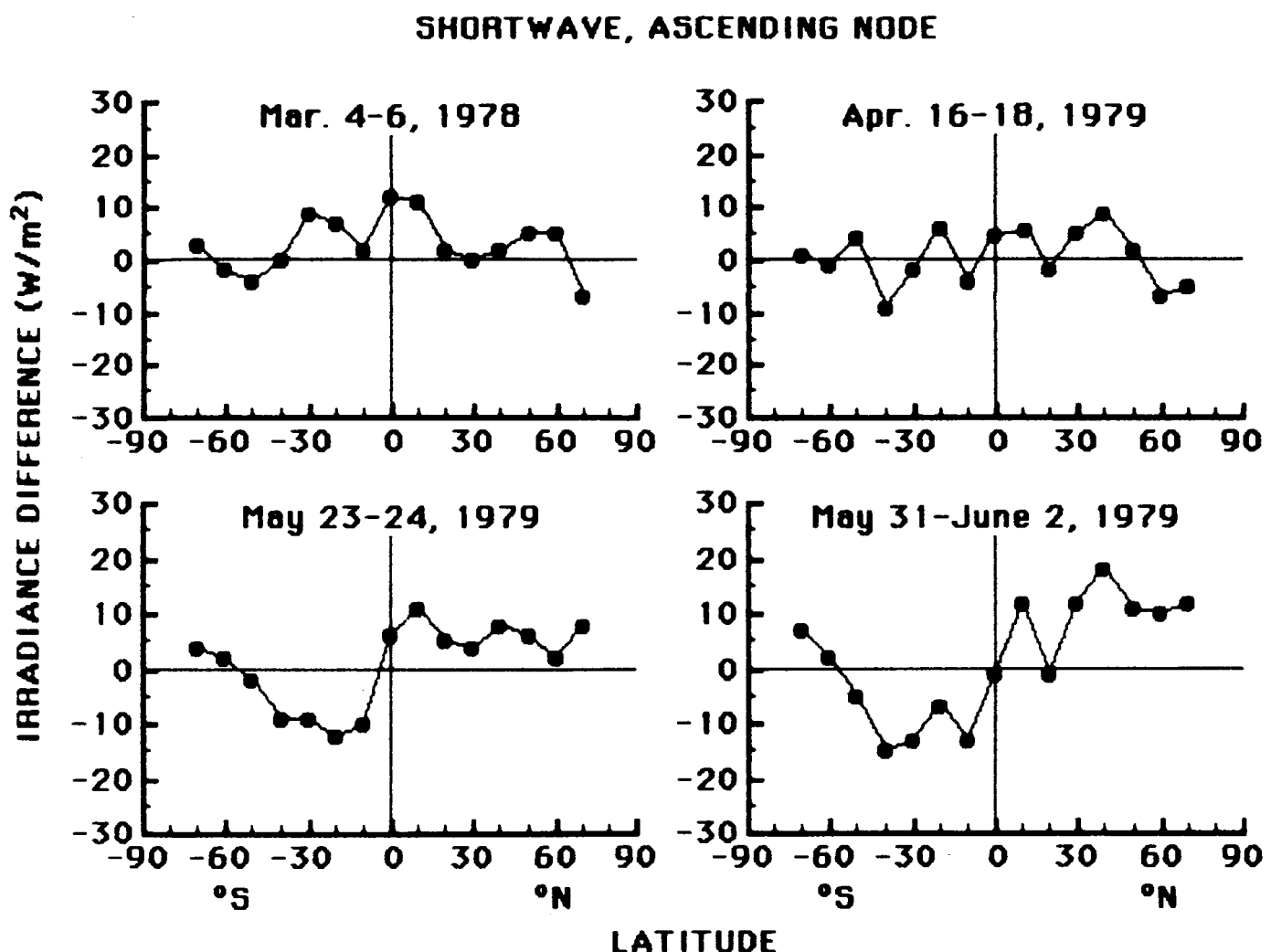


Fig. 4(b). Same as Fig. 4(a).

SHORTWAVE, ASCENDING NODE

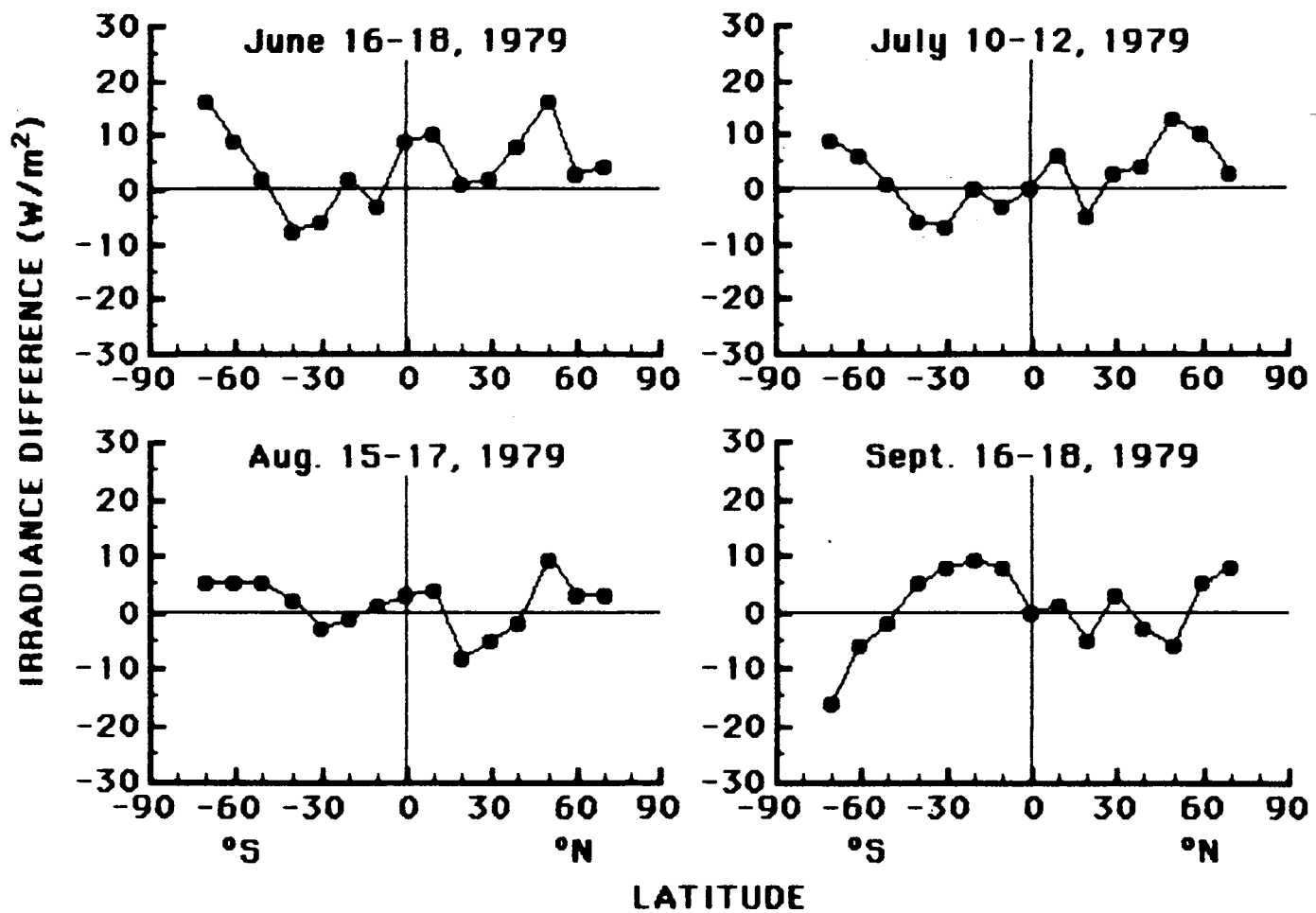


Fig. 4(c). Same as Fig. 4(a).

SHORTWAVE, ASCENDING NODE

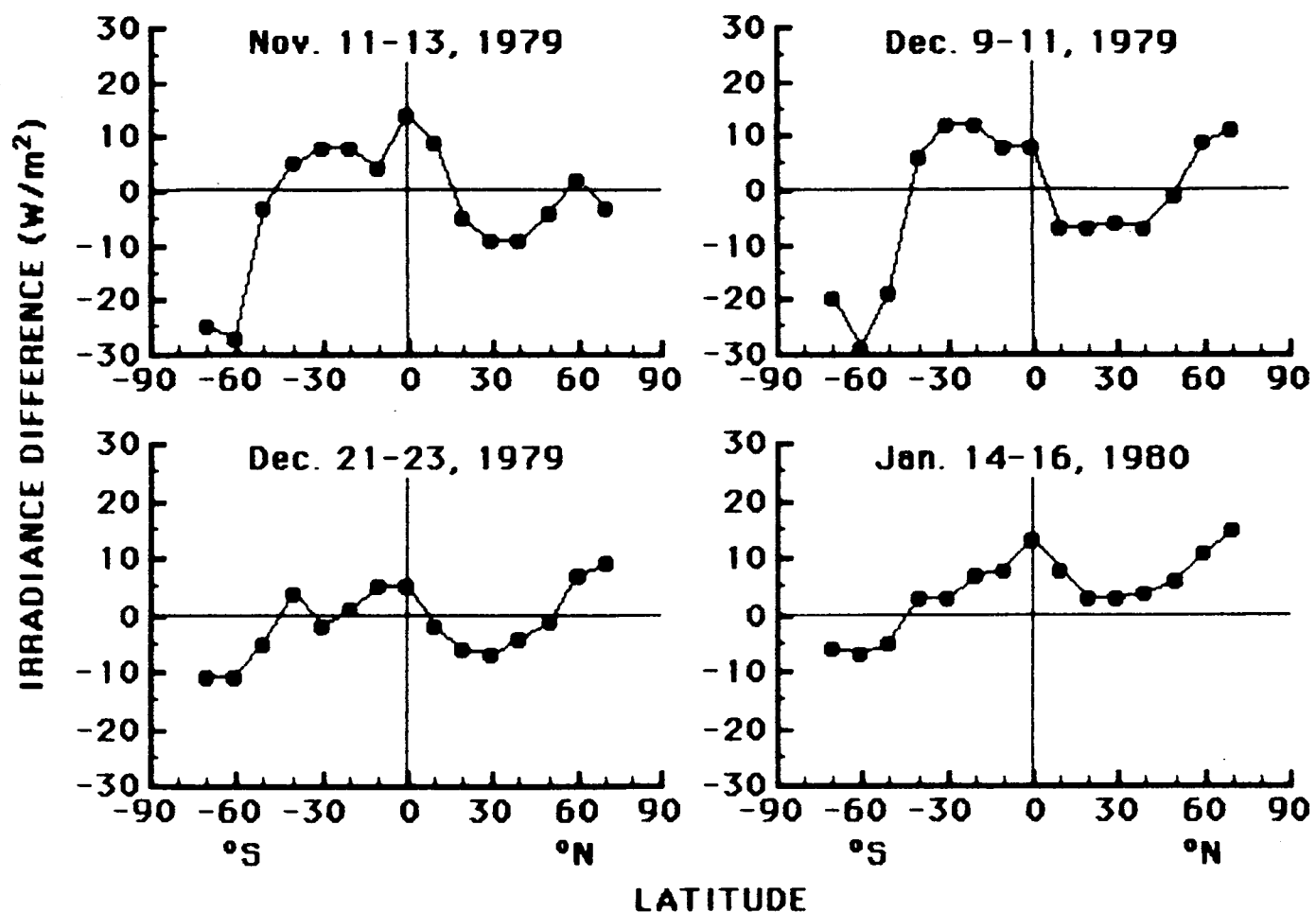


Fig. 4(d). Same as Fig. 4(a).

SHORTWAVE, ASCENDING NODE

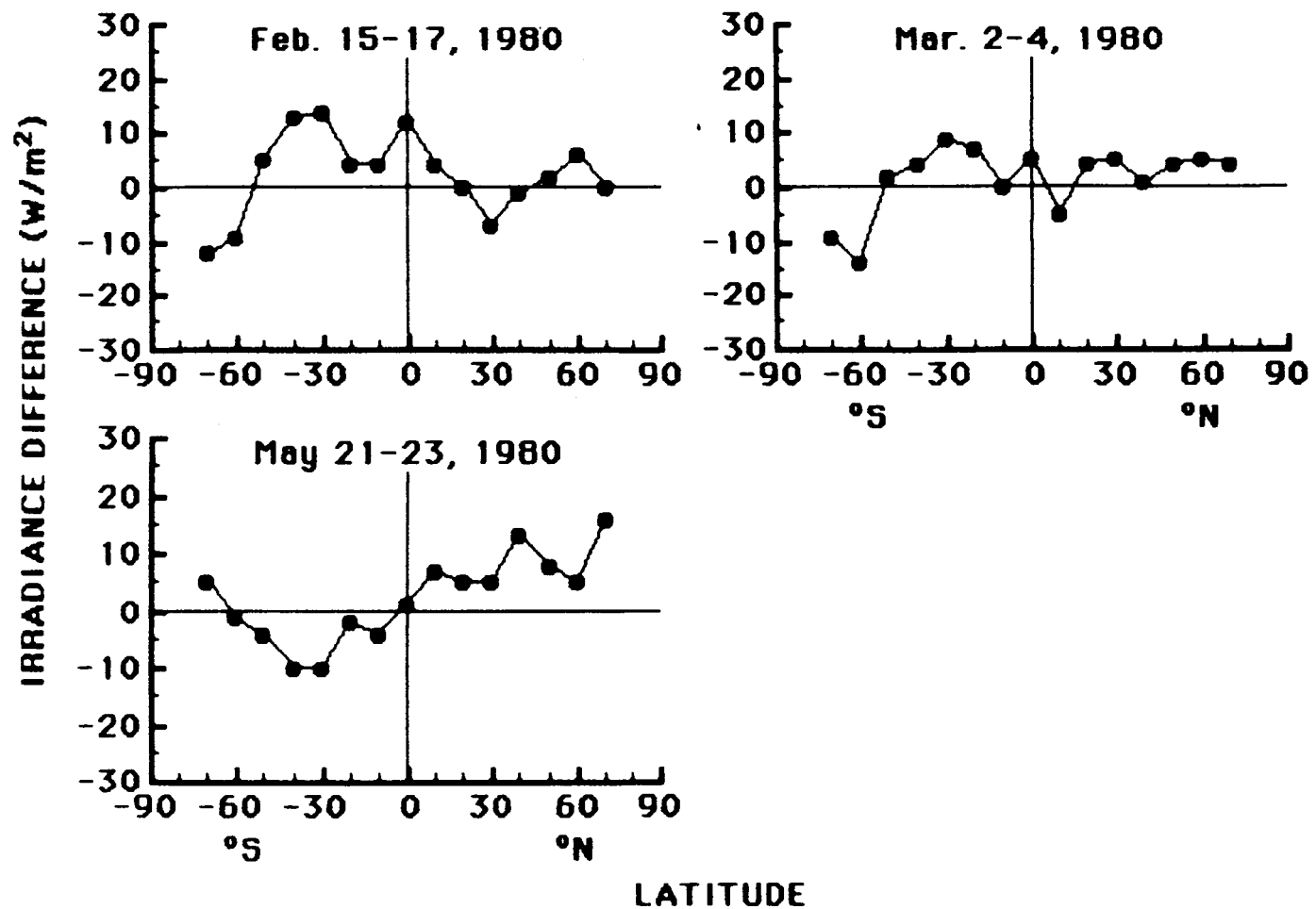


Fig. 4(e). Same as Fig. 4(a).

LONGWAVE STATISTICS

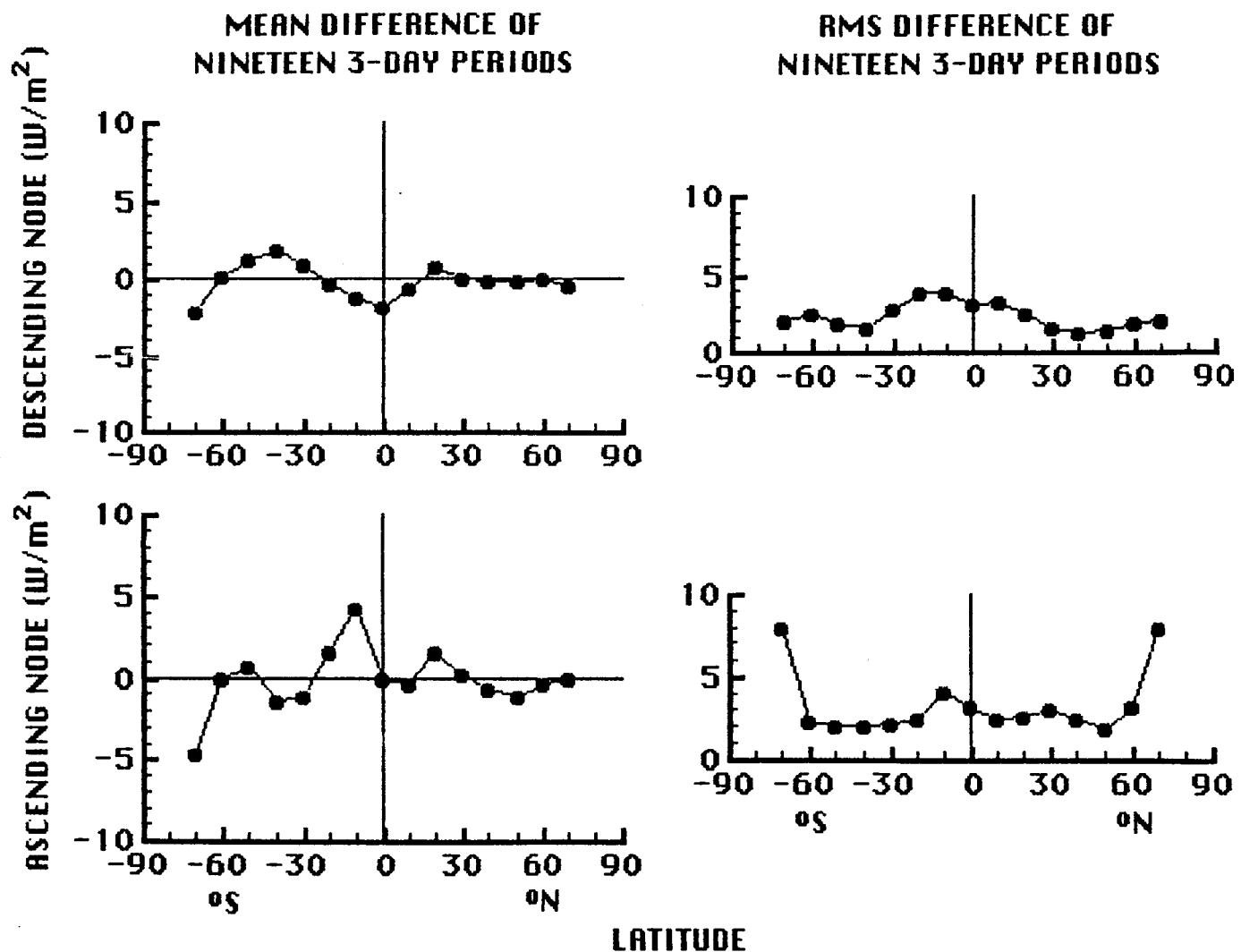


Fig. 5. Statistical summary of the nineteen 3-day periods of longwave differences shown in Fig. 1(a-e) and Fig. 2(a-e). The mean irradiance difference and associated RMS difference are plotted as a function of latitude for the descending node (upper graphs) and the ascending node (lower graphs).

SHORTWAVE STATISTICS

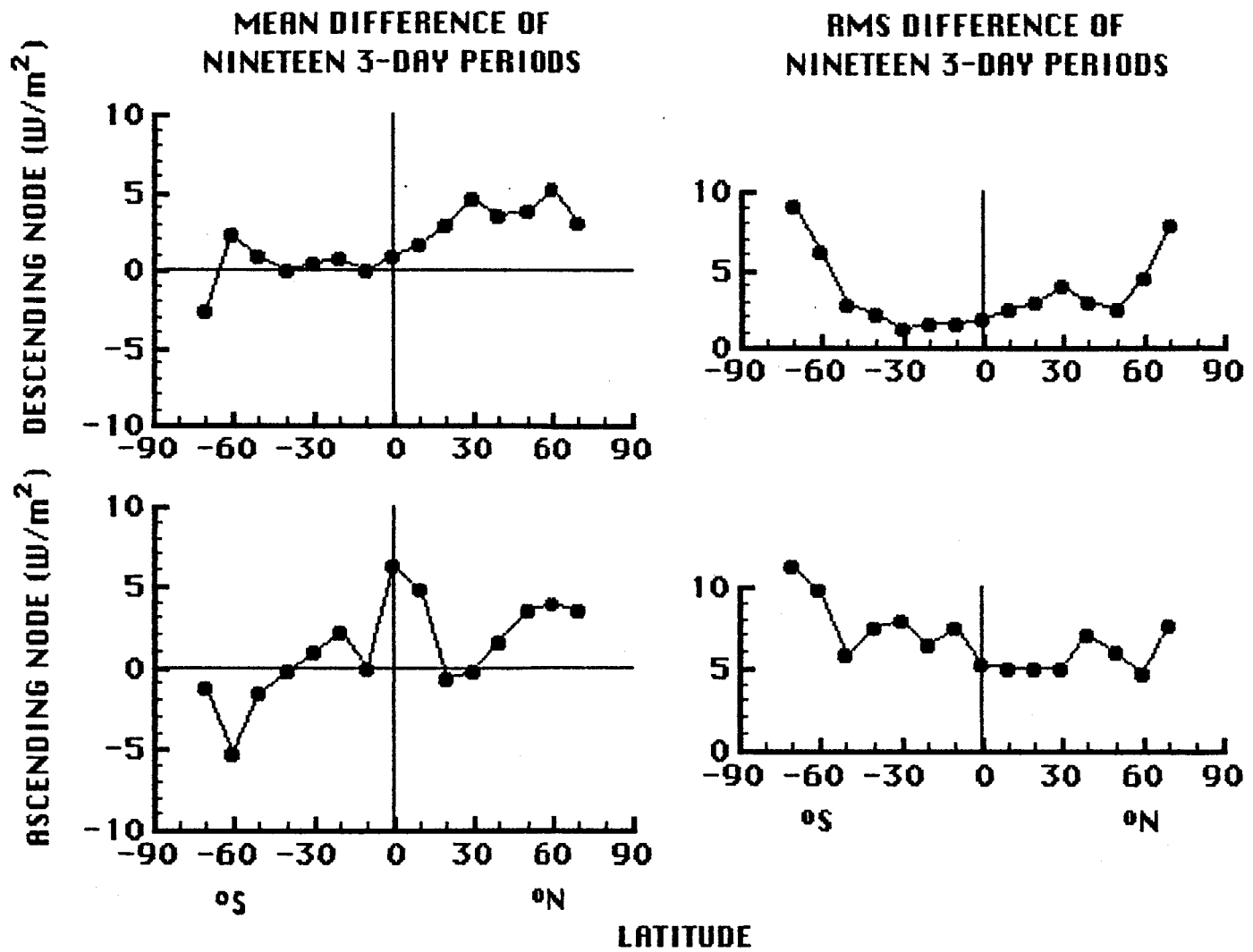


Fig. 6. Statistical summary of the nineteen 3-day periods of shortwave differences shown in Fig. 3(a-e) and Fig. 4(a-e). The mean irradiance difference and associated RMS difference are plotted as a function of latitude for the descending node (upper graphs) and the ascending node (lower graphs).